nature portfolio

https://doi.org/10.1038/s41929-022-00806-2

Supplementary information

Oxygenate-based routes regulate syngas conversion over oxide–zeolite bifunctional catalysts

In the format provided by the authors and unedited

Supplementary Information

Oxygenate-based Routes Regulate Syngas Conversion over Oxide-Zeolite Bifunctional Catalysts

Yi Ji[1,2,3], Pan Gao[1,3], Zhenchao Zhao[1], Dong Xiao[1], Qiao Han[1,2], Hongyu Chen[1,2], Ke Gong[1], Kuizhi Chen[1], Xiuwen Han[1], Xinhe Bao[1], and Guangjin Hou[1,*]

[1]State Key Laboratory of Catalysis, National Laboratory for Clean Energy, 2011-Collaborative Innovation Center of Chemistry for Energy Materials, Dalian Institute of Chemical Physics, Chinese Academy of Sciences, Zhongshan Road 457, Dalian 116023, China

[2]University of Chinese Academy of Sciences, Beijing 100049, China

[3]These authors contributed equally: Yi Ji, Pan Gao.

*e-mail: ghou@dicp.ac.cn

Supplementary Figures and Tables

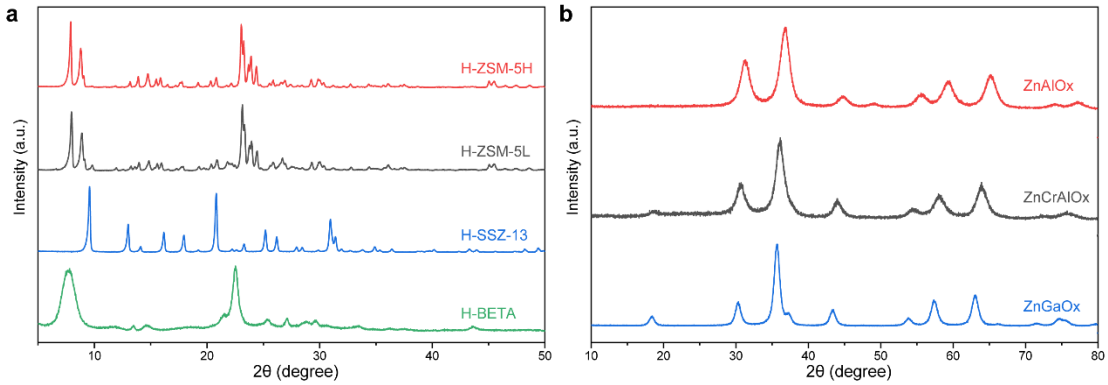

Supplementary Figure 1. Powder X-Ray Diffraction (PXRD) profiles: a, zeolites: H-ZSM-5H, H-ZSM-5L, H-SSZ-13 and H-BETA; **b**, spinel-structure oxides: $ZnAlO_x$, $ZnCrAlO_x$ and $ZnGaO_x$.

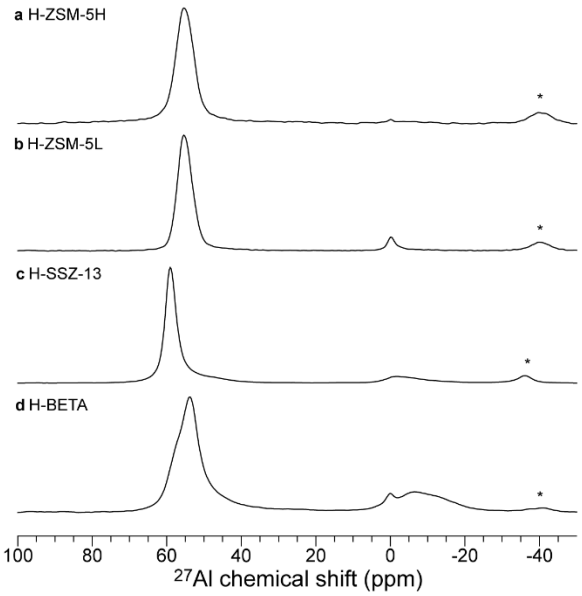

Supplementary Figure 2. ^{27}Al MAS NMR spectra of different zeolites: a, H-ZSM-5H, **b**, H-ZSM-5L, **c**, H-SSZ-13 and **d**, H-BETA. The major peaks located at around 60 ppm indicate tetrahedrally coordinated Al atoms on the framework, while minor signals at around 0 ppm reflect slight dealumination of the samples. Asterisks in spectra denote spinning sidebands.

Supplementary Table 1. Textural properties of H-ZSM-5 determined by N_2 physisorption.

Zeolite	S_{BET}[a] ($m^2 \cdot g^{-1}$)	S_{micro}[b] ($m^2 \cdot g^{-1}$)	$S_{external}$[c] ($m^2 \cdot g^{-1}$)	V_{total}[d] ($cm^3 \cdot g^{-1}$)	V_{micro}[e] ($cm^3 \cdot g^{-1}$)
H-ZSM-5H	344	226	118	0.23	0.13
H-ZSM-5L	313	229	84	0.19	0.12

[a]BET surface area.

[b]Micropore area calculated by the *t*-plot method.

[c]External surface area calculated by the *t*-plot method.

[d]Total pore volume.

[e]Micropore volume calculated by the *t*-plot method.

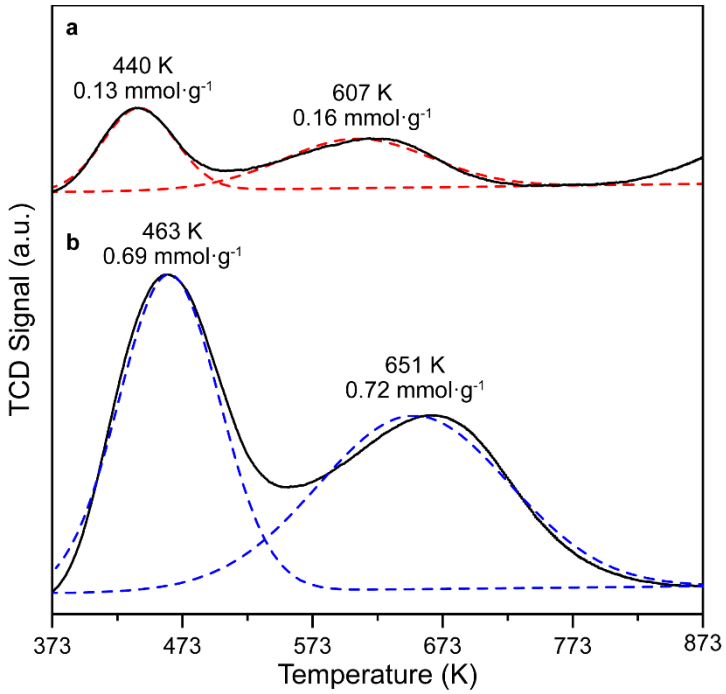

Supplementary Figure 3. NH_3-TPD profiles of H-ZSM-5: a, H-ZSM-5H and **b**, H-ZSM-5L. The total acid site density of H-ZSM-5L is about five times that of H-ZSM-5H, which is consistent with the elemental analysis.

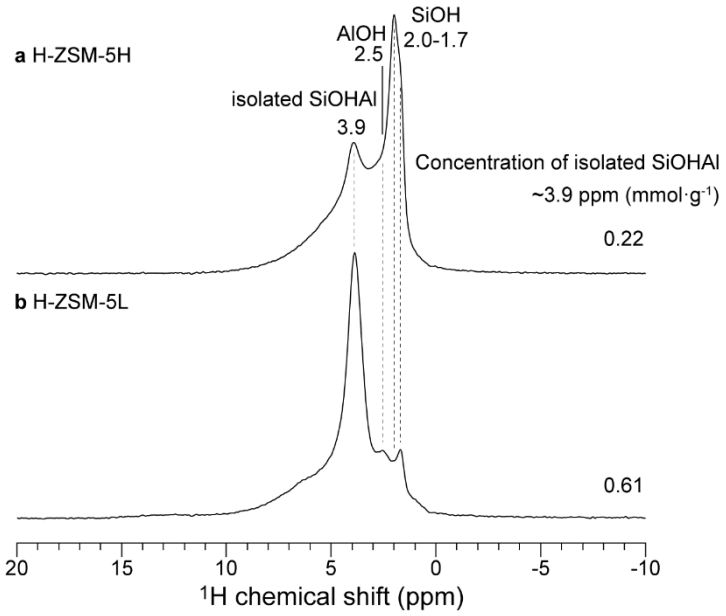

Supplementary Figure 4. ^{1}H MAS NMR spectra of H-ZSM-5: a, H-ZSM-5H and **b**, H-ZSM-5L. The quantity of isolated Si-OH-Al was calculated according to the integral area of the peaks at around 3.9 ppm and corresponding sidebands in ^{1}H MAS NMR spectra. The broad peaks at 5-8 ppm[1,2] and 12-15 ppm[3] have been assigned to kinds of hydrogen-bond species, some of which can also contribute to the BAS in H-ZSM-5. The amount of isolated BAS in H-ZSM-5H and H-ZSM-5L is 0.22 and 0.61 mmol·g^{-1}, respectively.

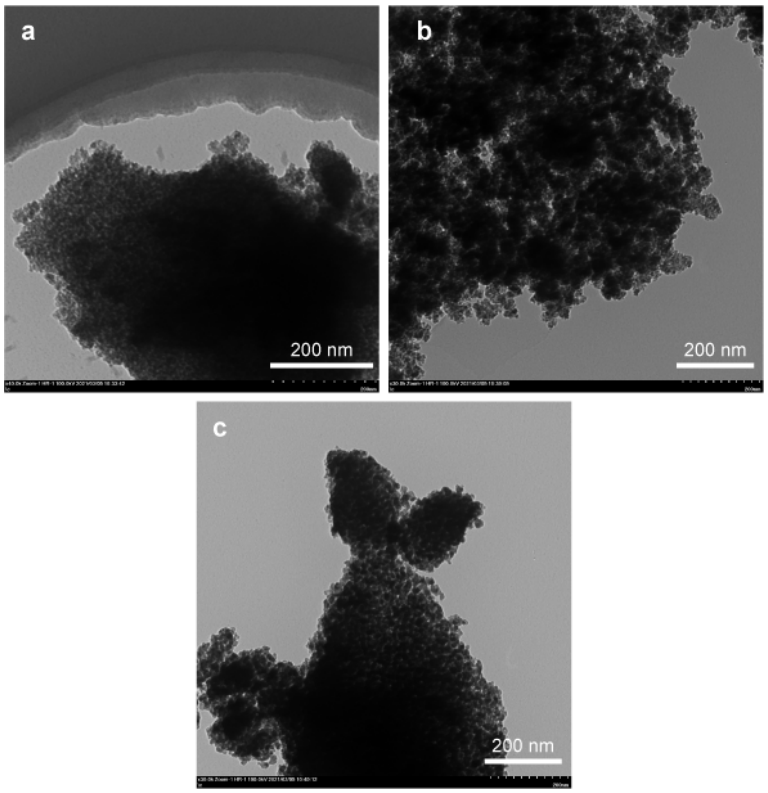

Supplementary Figure 5. TEM images of different oxides: a, $ZnAlO_x$, **b**, $ZnCrAlO_x$ and **c**, $ZnGaO_x$.

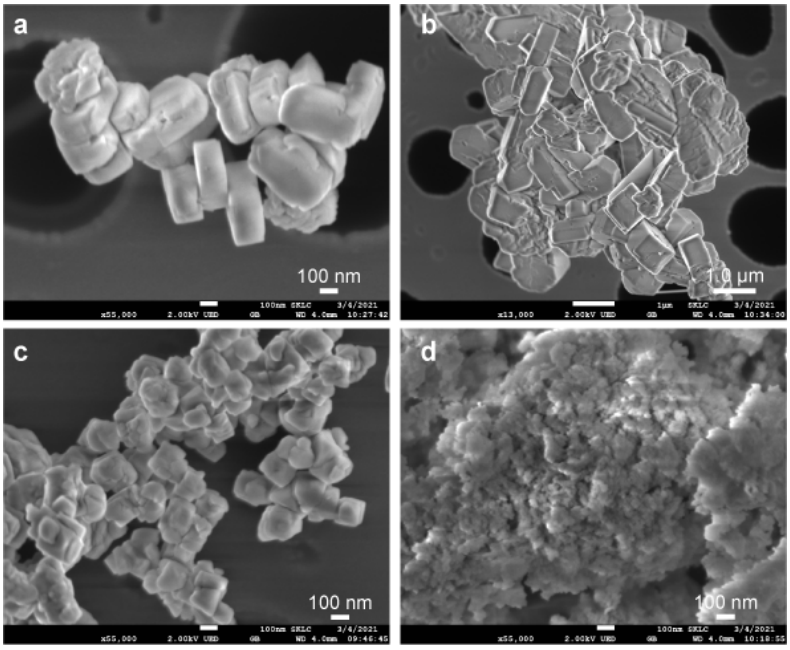

Supplementary Figure 6. SEM images of different zeolites: a, H-ZSM-5H, **b**, H-ZSM-5L, **c**, H-SSZ-13 and **d**, H-BETA.

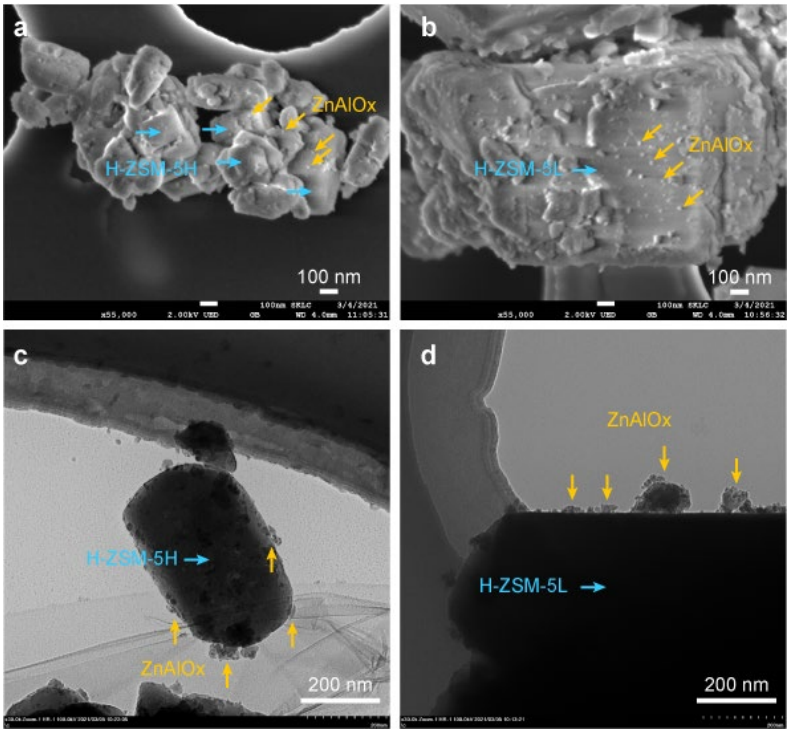

Supplementary Figure 7. SEM and TEM images of $ZnAlO_x$/H-ZSM-5 composite catalysts: SEM images of **a**, $ZnAlO_x$/H-ZSM-5H and **b**, $ZnAlO_x$/H-ZSM-5L; TEM images of **c**, $ZnAlO_x$/H-ZSM-5H and **d**, $ZnAlO_x$/H-ZSM-5L.

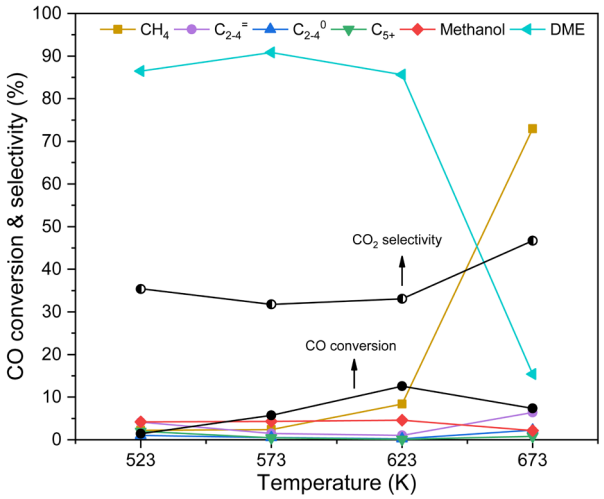

Supplementary Figure 8. Catalytic performances for syngas conversion over $ZnAlO_x$ at various temperature from 523 to 673 K. Reaction conditions: H_2/CO=1, 2.5 MPa, space velocity = 2000 $ml \cdot h^{-1} \cdot g_{cat}^{-1}$. Selectivities of MeOH, DME and hydrocarbons were calculated on a molar carbon basis by excluding CO_2 in the products.

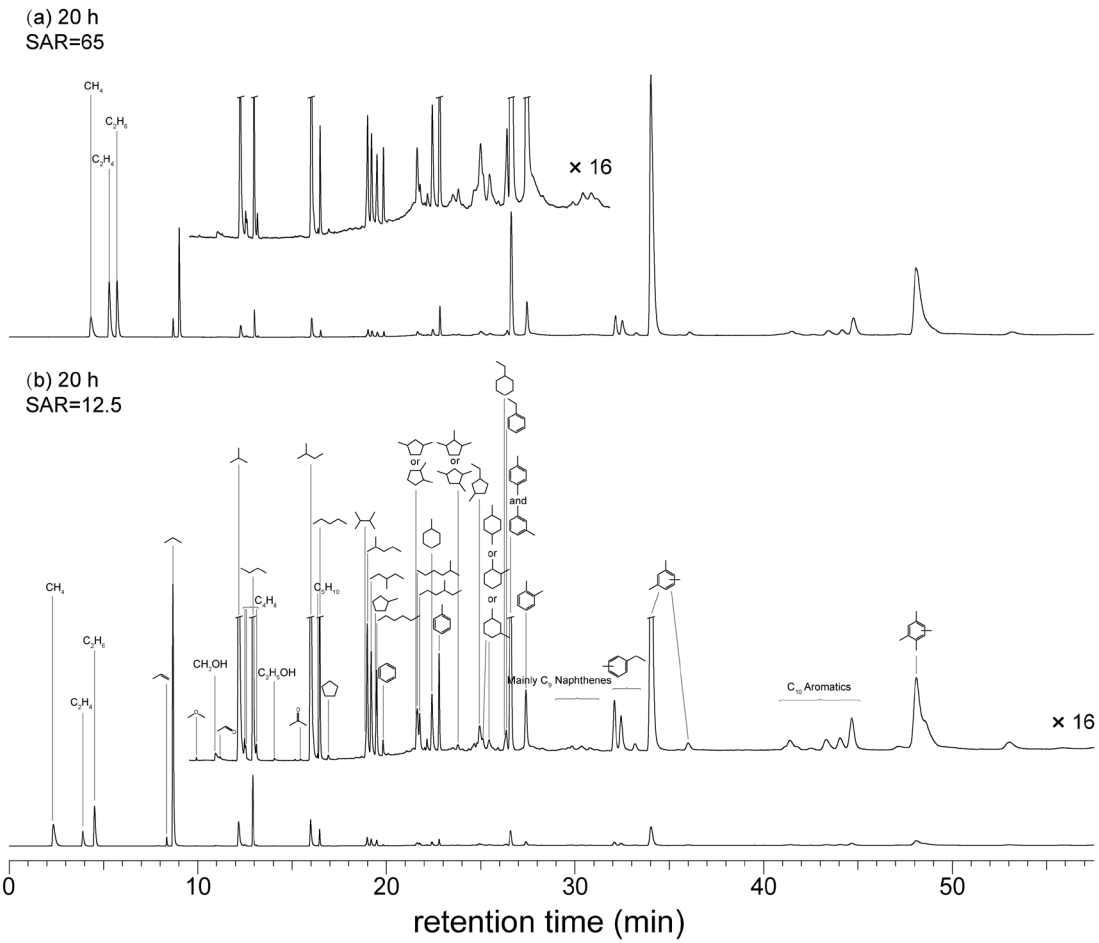

Supplementary Figure 9. GC-FIDs for the effluent products produced by $ZnAlO_x$/H-ZSM-5 catalysts: a, $ZnAlO_x$/H-ZSM-5H and **b**, $ZnAlO_x$/H-ZSM-5L after 20 h TOS. Reaction conditions: 573K, $H_2/CO=1$, 2.5 MPa, Space velocity = 1000 $ml \cdot h^{-1} \cdot g_{cat}^{-1}$. Different species are labelled according to GC-MS analysis (Supplementary Fig. 25).

Supplementary Note 1.

Hydrogen transfer (HT) process can be qualitatively evaluated using hydrogen transfer index (HTI), defined as the ratio of paraffines to olefins formed in MTH reactions[4-6]. However, original HTI is unsuitable in syngas conversion for the prevailing hydrogenation. Herein, an alternative index, named aromatics hydrogen transfer index (AHTI), is used, calculated as follows:

$$\mathrm{AHTI} = \frac{3 \times n_{\mathrm{outlet}}C_nH_{2n-6}}{n_{\mathrm{outlet}}C_nH_{2n+2}} \quad (1)$$

where $n_{\mathrm{outlet}}C_nH_{2n-6}$ and $n_{\mathrm{outlet}}C_nH_{2n+2}$ represent the moles of effluent alkyl-substituted benzenes and paraffines, respectively. Considering the low resolution for C_{6+} hydrocarbons as shown in Supplementary Fig. 9, all C_{6+} hydrocarbons have been calculated as chained C_6 paraffins to obtain a lower limit of AHTI. During the calculation of AHTI, we consider that reactive C_1 intermediates, methanol ($CH_2(H_2O)$) and/or ketene ($CH_2(CO)$) produce olefins $(CH_2)_n$, which disproportionate to form aromatics (C_nH_{2n-6}) and paraffines (C_nH_{2n+2})[4]. There ought to be three moles paraffins formed through HT to form one mole aromatics, if *barely* the HT process is responsible for producing aromatics. AHTI higher than 1 suggests other processes occur and reduce the H/C ratio in products when no carbon deposition processes occur in the catalysts.

Such an analysis is well suited for syngas conversion over bifunctional catalysts with high carbon balance during the steady state. AHTI of 3.2 with carbon balance (>95%) was achieved after 20 h on-line reaction at 573 K over $ZnAlO_x$/H-ZSM-5H (carbon balance was above 85% since 4 h TOS). There must be other processes besides HT responsible for producing so many highly unsaturated products. “de_H_2 and aromatization” process is unreasonable for the production of H_2 under high-pressure H_2 atmosphere and contradicts with the prevailing hydrogenation process (reverse process to dehydrogenation) to produce paraffins observed in experiments. On the other hand, above analysis strongly supports a vigorous participation of oxygenates-based routes and dehydration processes proposed in the text.

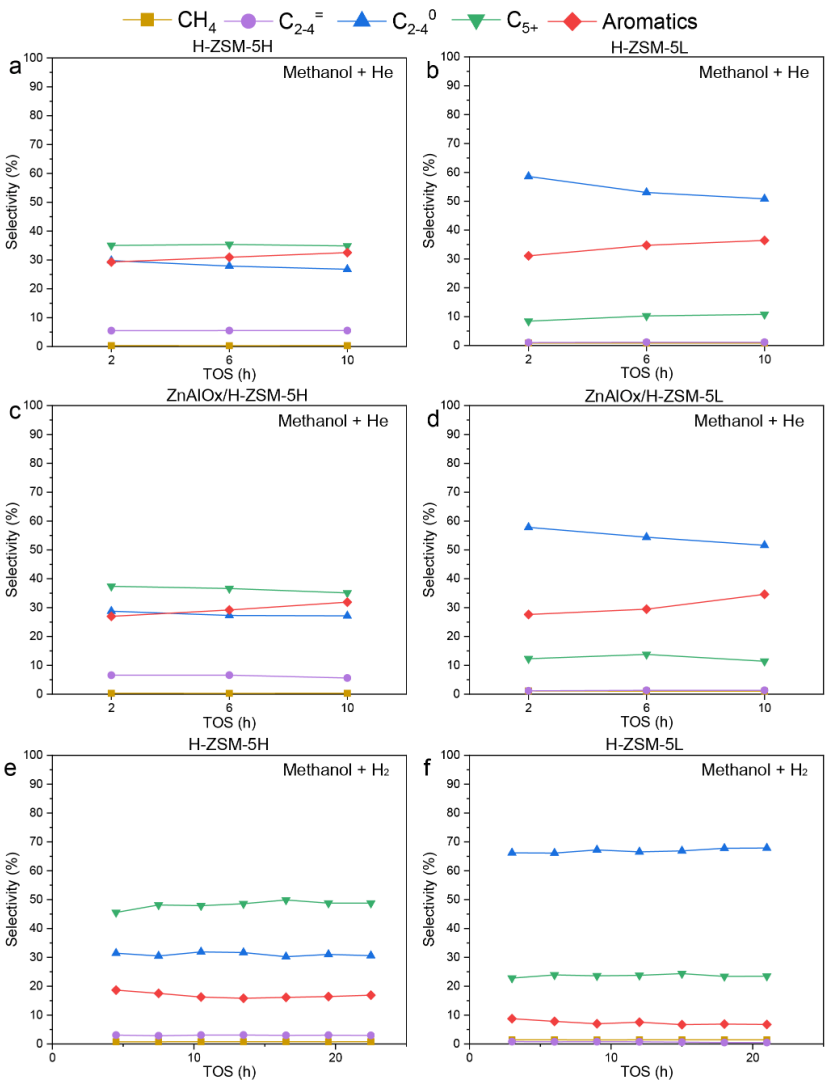

Supplementary Figure 10. Catalytic performance for methanol conversion with He or H_2 cofeeding over H-ZSM-5 and $ZnAlO_x$/H-ZSM-5. Time-on-stream selectivity of **a**, H-ZSM-5H, **b**, H-ZSM-5L, **c**, $ZnAlO_x$/H-ZSM-5H, and **d**, $ZnAlO_x$/H-ZSM-5L for methanol conversion under He flow. Reaction conditions: 573 K, 22 kPa MeOH balanced with 1.25 MPa of He, space velocity = 2000 $ml \cdot h^{-1} \cdot g_{zeo}^{-1}$. Time-on-stream selectivity of **e**, H-ZSM-5H, **f**, H-ZSM-5L for methanol conversion under H_2 flow. Reaction conditions: 573 K, 22 kPa MeOH balanced with 1.25 MPa of H_2, space velocity = 1000 $ml/h^{-1} \cdot g_{cat}^{-1}$ for composite catalysts (mass ratio of oxides/zeolites = 1:1) or space velocity = 2000 $ml \cdot h^{-1} \cdot g_{zeo}^{-1}$ for zeolites alone. The conversion is around 100 % on all different catalysts with a selectivity to DME < 0.5% (not presented).

For both H-ZSM-5 catalysts in methanol conversion under He atmosphere (**a** and **b**), paraffins are the major products (C_2-C_{5+} for H-ZSM-5H and C_{2-4}^0 for H-ZSM-5L) along with moderate amounts of aromatic products (~35%), consistent with a high degree of hydrogen-transfer (HT) reactions, i.e., 3 mol of saturated alkanes are simultaneously formed with 1 mol of aromatics produced. Further, $ZnAlO_x$ oxide does not involve methanol conversion processes under He atmosphere (**a**-**d**). For methanol conversion under H_2 atmosphere, the hydrogenation reactions strongly truncate HT, thus leading to higher paraffin selectivity, but lower aromatic selectivity (**e**, ~ 17 % for H-ZSM-5H; **f**, ~ 7 % for H-ZSM-5L).

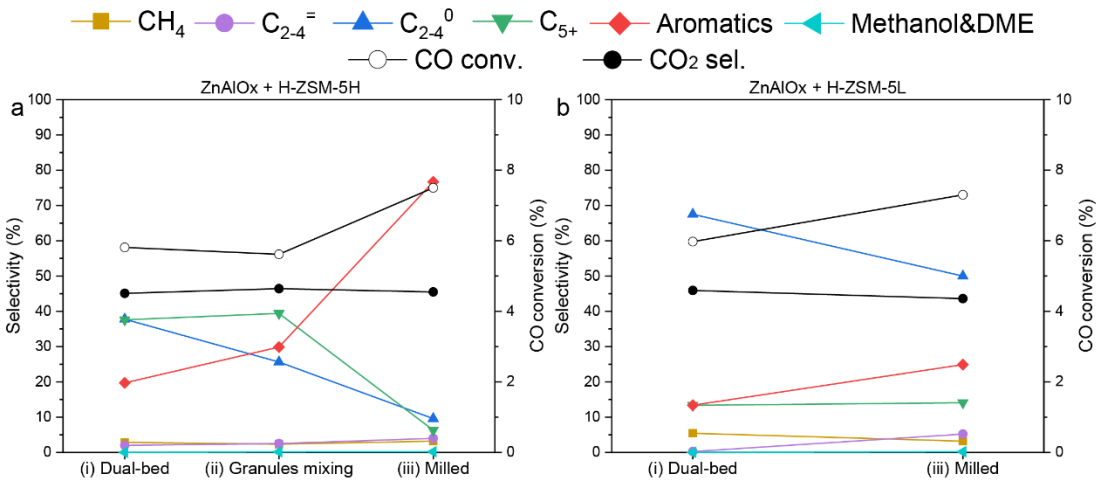

Supplementary Figure 11. Effect of the proximity of the $ZnAlO_x$ and H-ZSM-5 components on the catalytic performance for syngas conversion. The $ZnAlO_x$ and H-ZSM-5 are mixed through different methods including: (i) dual-bed, (ii) granule mixing (300 - 450 μm), and (iii) milled. Conversion and selectivity are presented for the composite catalysts with **a**, H-ZSM-5H and **b**, H-ZSM-5L components, respectively. Reaction conditions: 573 K, H_2/CO=1, 2.5 MPa, space velocity = 1000 $ml \cdot h^{-1} \cdot g_{cat}^{-1}$, TOS = 20 h. The mass ratio of oxides/zeolites = 1:1. Selectivities of MeOH, DME and hydrocarbons were calculated on a molar carbon basis by excluding CO_2 in the products.

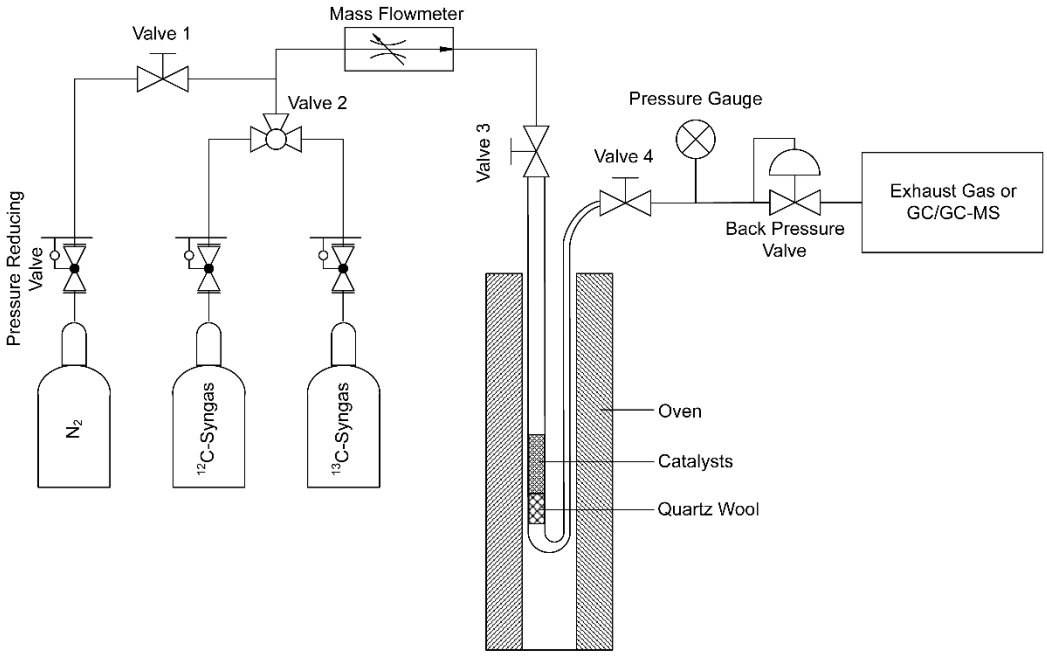

Supplementary Figure 12. Schematic diagram of the experimental device for quasi-in-situ NMR-GC/GC-MS study on the syngas conversion.

The basic experimental device is a home-built high-pressure fixed-bed catalytic reactor. In order to simultaneously monitor the reaction products and adsorbed species on the catalysts, we've adopted the "quench" method originally developed by Haw et al.[7] and adapted to our reactor. At predetermined reaction intervals, the gas phase products were routed into the GC/GC-MS for online analysis, meanwhile the oven was simultaneously removed and the reactor was quickly immersed into liquid nitrogen to quench the reaction (this process should last as short as possible to ensure the consistency of NMR and GC/GC-MS analysis), so that highly reactive intermediates on the catalysts can be captured while maintain their original states. Subsequently, the reactor was sealed, after waiting for recovery to room temperature, and further transferred into a glovebox filled with Ar for further NMR sample packing.

Supplementary Table 2. Overview of the species assigned by ssNMR and GC-MS in this work. The chemical shifts of different carbons and protons are shown in black and blue, respectively.

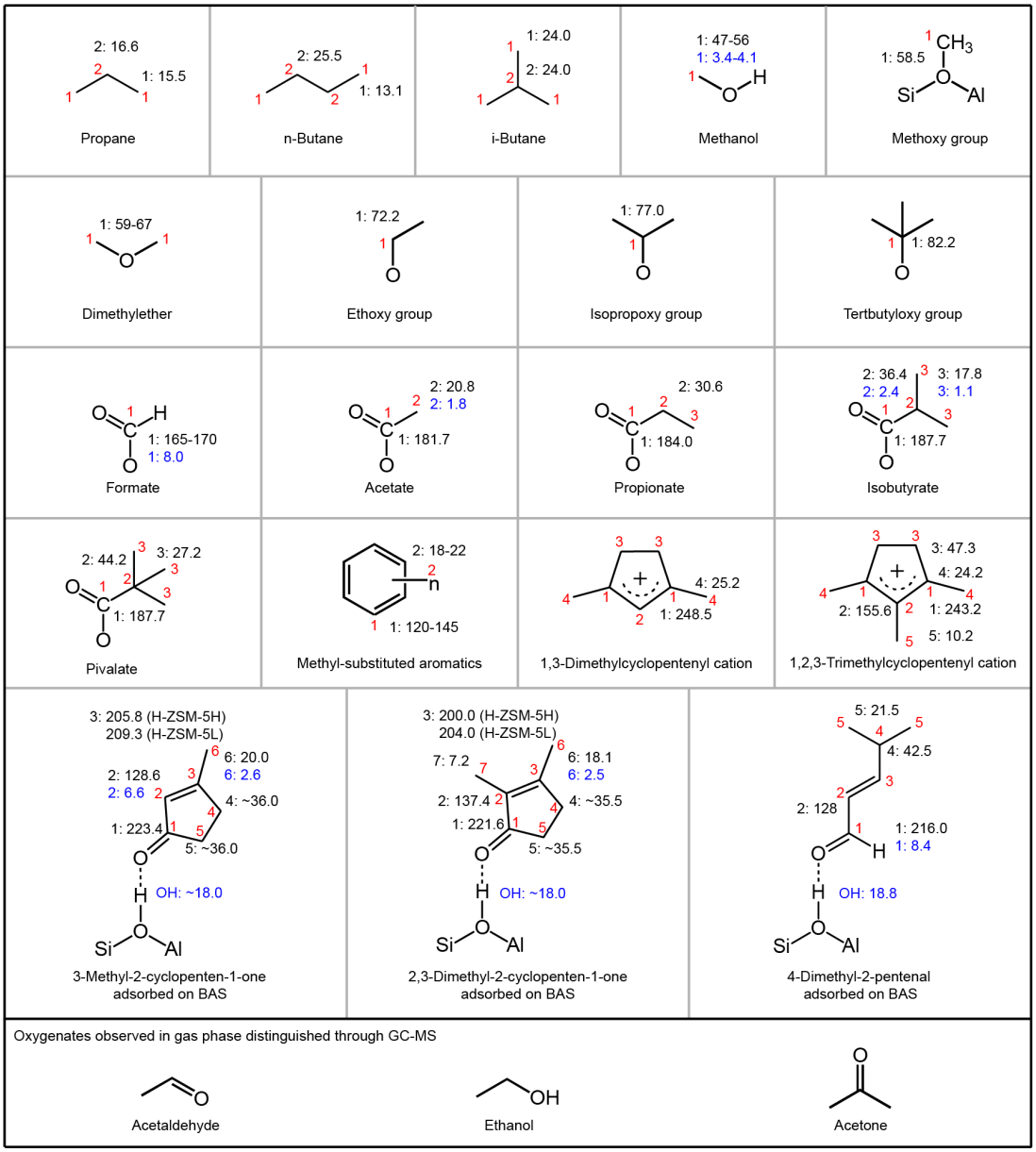

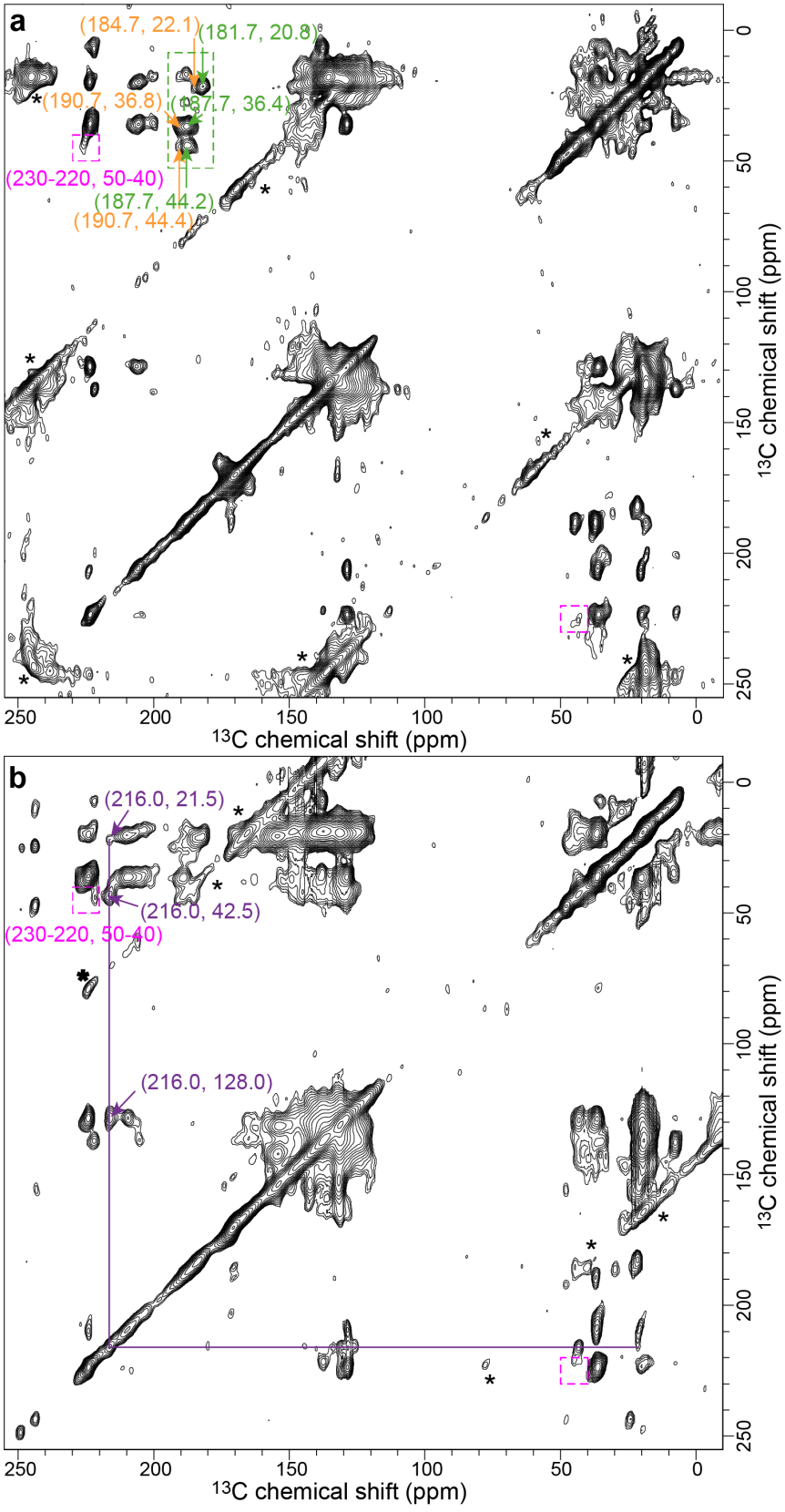

Supplementary Figure 13. Full ^{13}C-^{13}C CORDxy4 correlation MAS NMR spectra. a, $ZnAlO_x$/H-ZSM-5H and **b**, $ZnAlO_x$/H-ZSM-5L catalysts after ^{13}C-syngas reaction for 4 h. Tailored spectra are shown as Fig. 3**a-b** in the text. Asterisks denote spinning sidebands.

Supplementary Note 2.

Assignments for carboxylates and carboxylic acids. As presented in the *green* frame in Supplementary Fig. 13**a** and Fig. 14**a** and the strip-shape correlation peaks in Fig. 4, the carboxyl groups of the trapped species in $ZnAlO_x$/H-ZSM-5H are presented with a distribution in chemical shifts, e.g., the correlated signals at (181.7 ppm, 20.8 ppm) and (184.7 ppm, 22.1 ppm) (Supplementary Fig. 13**a**). Similar observations are also found for the correlated signals at (187.7 ppm, 44.2 ppm) and (190.7 ppm, 44.4 ppm), as well as (187.7 ppm, 36.4 ppm) and (190.7 ppm, 36.8 ppm). One possible explanation is that the signals at relatively low field (*orange* arrow) belong to carboxylic acids, while the signals at higher field (*green* arrow) belong to carboxylates.

Assignments for the α,β-unsaturated aldehyde adsorbed on BAS. As shown for the *purple* line in Supplementary Fig. 13**b**, correlated ^{13}C signals have been found at 21.5, 42.5, 128.0, and 216.0 ppm, which have been assigned to different carbons in α,β-unsaturated aldehyde adsorbed on BAS in the text. The basis is as follows: (1) The peak at 216.0 ppm showed strong correlation to the ^{1}H signal at 18.8 ppm (Supplementary Fig. 14**b**), which is typical for the aldehyde/ketone adsorbed on BAS in H-ZSM-5[8-11]. (2) correlations between 18.8 and 8.4 (^{1}H) ppm were found in the ^{1}H-^{1}H DQ-SQ experiment with short (100 μs) DQ excitation time (Supplementary Fig. 15), which means these two proton must be close in space. One possible assignment is aldehyde adsorbed on BAS. The peak at 18.8 ppm belongs to the H of BAS, while the peak at 8.4 ppm belongs to the H in the original -CHO. (3) The peak at 216.0 ppm was found correlated with the peak at 128.0 ppm in ^{13}C CP refocused INADEQUATE spectrum (Fig. 4), so this specie should be α,β-unsaturated aldehyde, such as 4-dimethyl-2-pentenal (Supplementary Table 2), adsorbed on BAS. Corresponding signal of C_β should be at 180-200 ppm which may overlap with the carboxyl groups in multi-carbon carboxylates.

Assignments for MCPenones with tertiary carbons. As presented in the *pink* frame in Supplementary Fig. 13**a-b**, the correlated signals between 220-230 and 40-50 ppm suggest other kinds of MCPenones with tertiary carbons have been produced (Supplementary Fig. 17 and Supplementary Table 3).

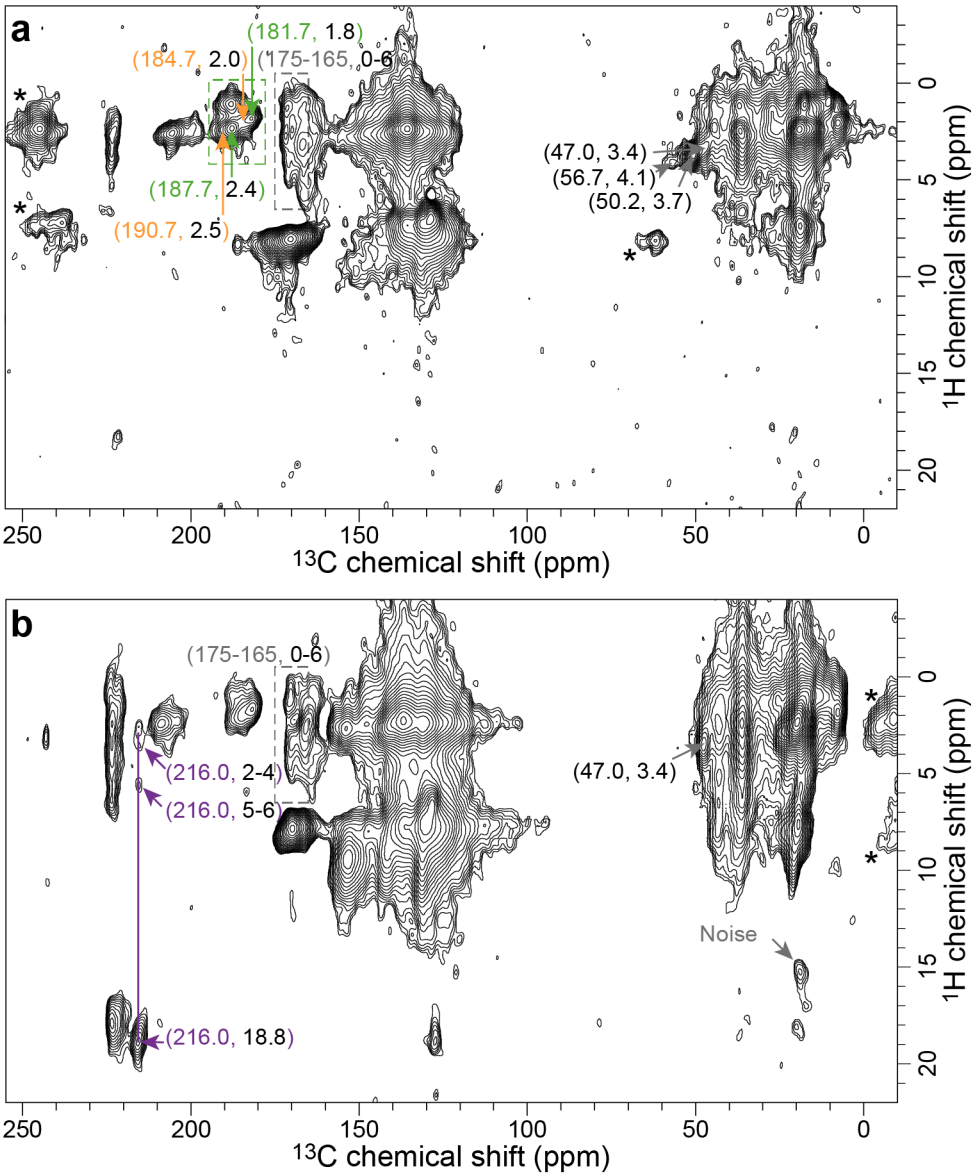

Supplementary Figure 14. Full ^{13}C{^{1}H} CP HETCOR MAS NMR spectra. a, $ZnAlO_x$/H-ZSM-5H and **b**, $ZnAlO_x$/H-ZSM-5L catalysts after ^{13}C-syngas reaction for 4 h. Tailored spectra are shown as Fig. 3**c-d** in the text. Asterisks denote spinning sidebands. The "noise" labelled at around 20 ppm in the ^{13}C dimension in **b** is due to the t_1 noise probably from MAS fluctuation and probe power variations.

Supplementary Note 3.

Assignments for methanol. As presented for the *grey* arrow in Supplementary Fig. 14**a-b**, correlated signals have been found between ^{13}C: 47-57 ppm and ^{1}H: 3.4-4.1 ppm, which supports our assignments for methanol in the text[12].

Explainations for the correlated ^{13}C-^{1}H signals for formates. As shown in the *grey* frame in Supplementary Fig. 14**a-b**, correlated signals have been found between ^{13}C: 165-170 ppm and ^{1}H: 0-6 ppm, which could be due to the proximity between formates and hydroxyl/methoxyl groups on the surface of oxides.

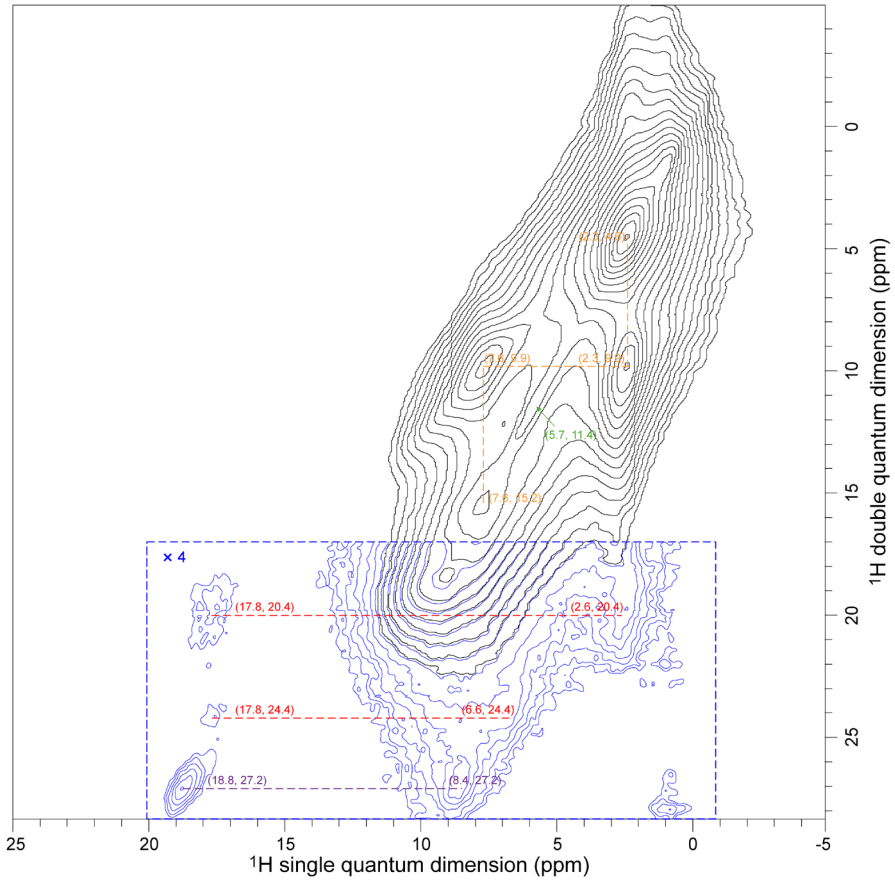

Supplementary Figure 15. ^{1}H-^{1}H DQ-SQ MAS NMR spectra for $ZnAlO_x$/H-ZSM-5L after 4 h ^{13}C-syngas conversion reaction. *Orange* line: methyl-substituted aromatics[13-15]. *Green* arrow: adsorbed olefines[12]. *Red* line: MCPenones adsorbed on BASs. *Purple* line: α,β-unsaturated aldehyde adsorbed on BASs.

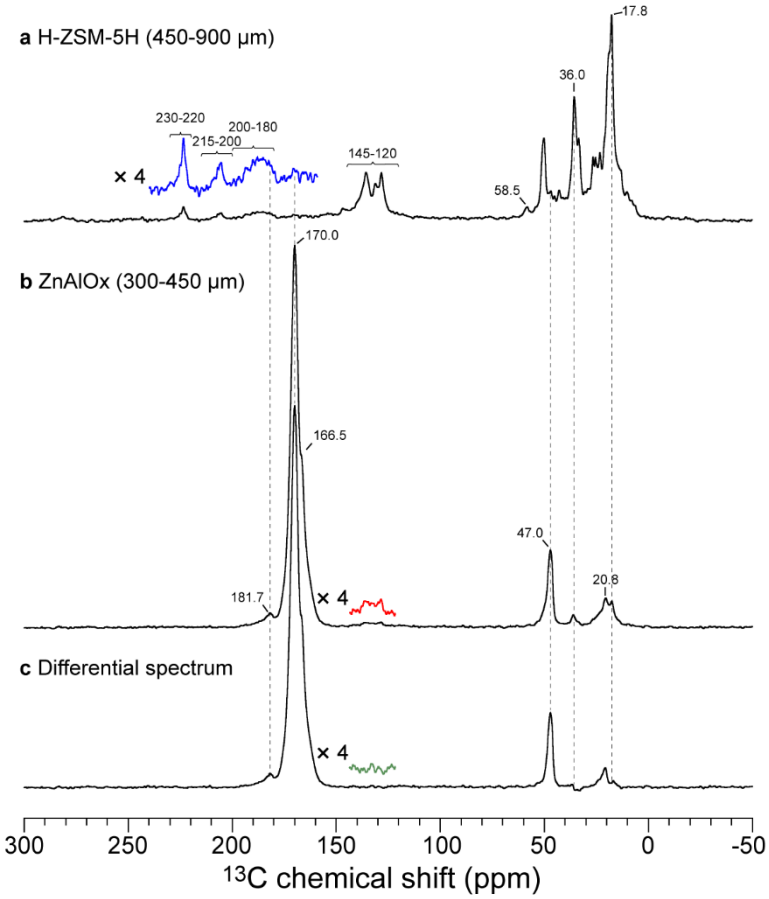

Supplementary Figure 16. ^{13}C CP MAS NMR spectra for the adsorbed species in the separated H-ZSM-5H and ZnAlO$_x$. a, sieved H-ZSM-5H and **b**, sieved ZnAlO$_x$. Differential spectrum is shown in **c** in a form of spectrum **b** minus scaled **a**, for removing signals from the trapped species in the smashed zeolites after reaction which could lead to the signals at 17.8, 36.0, and 120-145 ppm.

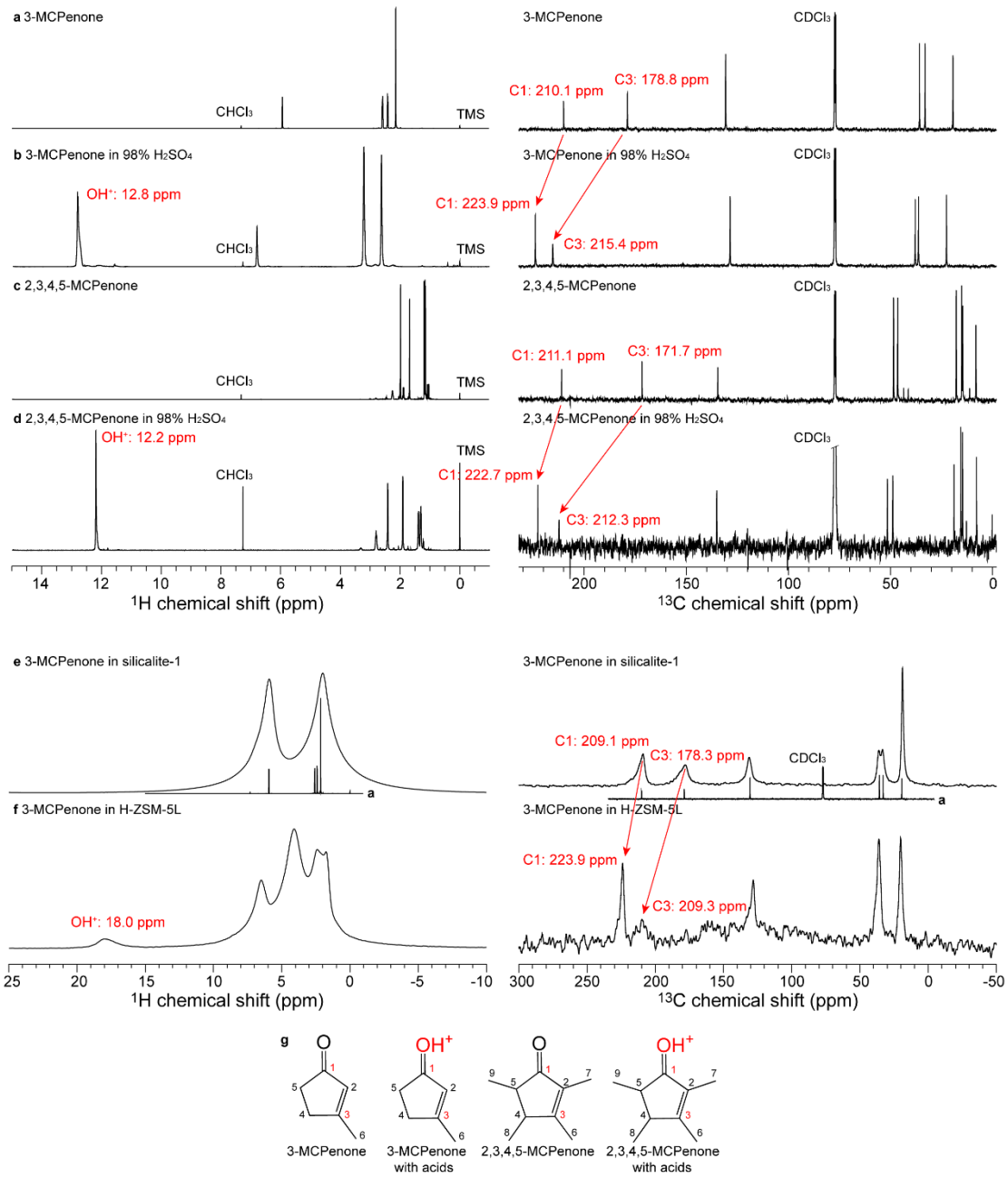

Supplementary Figure 17. ^{1}H and ^{13}C NMR spectra of the MCPenones in H_2SO_4 and zeolites. ^{1}H NMR spectra (reference: TMS at 0 ppm) for 3-Methyl-2-cyclopentene-1-one (3-MCPenone) in **a**, $CDCl_3$ or **b**, 98% H_2SO_4; 2,3,4,5-Tetramethyl-2-cyclopenteneone (2,3,4,5-MCPenone, majorly trans) in **c**, $CDCl_3$ or **d**, 98% H_2SO_4. Corresponding ^{13}C NMR spectra (reference: $CDCl_3$ at 77.16 ppm) are shown on the right side. ^{1}H MAS NMR spectra (reference: solid adamantane at 1.74 ppm) of 3-MCPenone in **e**, silicalite-1 and **f**, H-ZSM-5L. Corresponding ^{13}C CP MAS NMR spectra (reference: solid adamantane, CH, at 29.45 ppm) are shown on the right side. Liquid-state NMR spectra were acquired at 9.4 T. Solid-state NMR spectra were acquired at 12 kHz MAS and 9.4 T. Different MCPenone species are shown in **g**. The chemical shifts for different carbons and protons are provided in Supplementary Table 3.

Supplementary Table 3. Summary of ^{1}H and ^{13}C chemical shifts of the MCPenones[a] in H_2SO_4 and zeolites. Corresponding ^{1}H and ^{13}C NMR spectra are shown in Supplementary Fig. 17.

Species	C1	C2	C3	C4	C5	C6	C7	C8	C9	OH
3-MCPenone in $CDCl_3$	210.1	130.7 (5.9)	178.8	33.0 (2.6)	35.8 (2.4)	19.4 (2.2)	N/A	N/A	N/A	N/A
3-MCPenone in silicalite-1[b]	209.1	131.3 (5.9)	178.3	33.5	36.2	18.9	N/A	N/A	N/A	N/A
3-MCPenone in 98% H_2SO_4	223.9	128.5 (6.8)	215.4	36.2 (3.2)	37.8 (3.2)	22.6 (2.6)	N/A	N/A	N/A	(12.8)
3-MCPenone in H-ZSM-5L[b]	223.9	128.3 (6.5)	209.3	36.0 [d]	36.0	20.2	N/A	N/A	N/A	(18.0)
2,3,4,5-MCPenone[c] in $CDCl_3$	211.1	134.6	171.7	46.5	48.6	17.8	8.2	14.7	15.2	N/A
2,3,4,5-MCPenone in 98% H_2SO_4[b]	222.7	135.1	212.3	48.9	51.4	18.8	7.8	14.7	15.6	(12.2)

[a]Reference: ^{1}H: TMS at 0 ppm for liquid-state NMR; Adamantane at 1.74 ppm for solid-state NMR; ^{13}C: $CDCl_3$ at 77.16 ppm for liquid-state NMR; Adamantane (CH) at 29.45 ppm for solid-state NMR. ^{1}H chemical shifts are provided in parentheses below the linked carbon or OH for hydrogen bond with acids.

[b]Barely protons in OH and pontons bonded to C2 are provided in ^{1}H chemical shifts for limited resolution.

[c]^{13}C chemical shifts for trans-2,3,4,5-MCPenone (the major configuration) are provided

[d]C4 and C5 showed a single peak (FWMH: 3.5 ppm at 9.4 T) in the ^{13}C MAS NMR spectra for the close chemical shifts and a distribution of BASs.

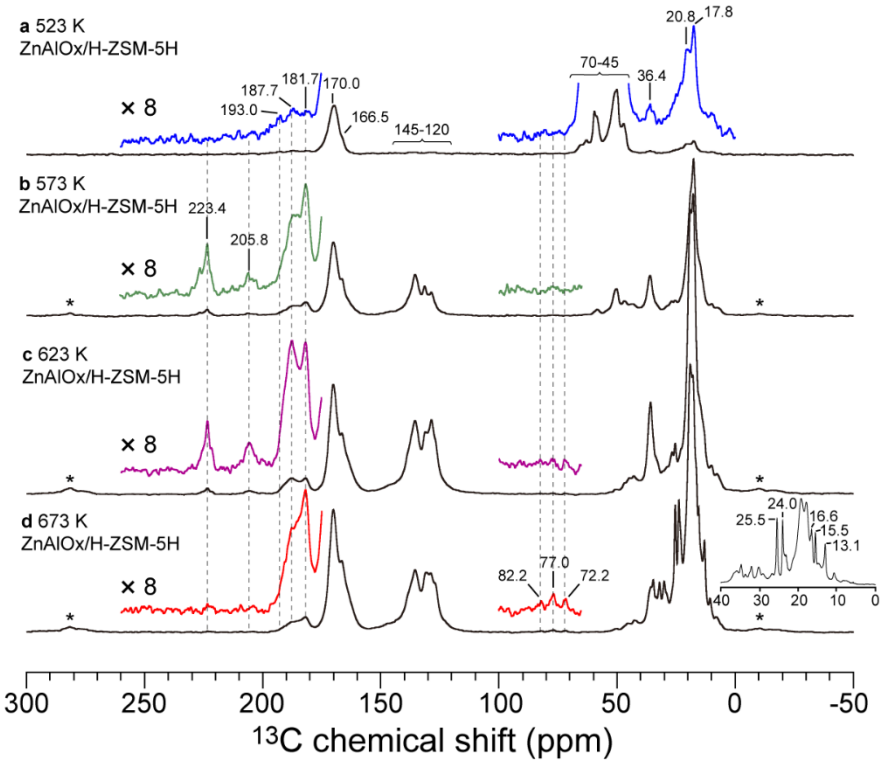

Supplementary Figure 18. ^{13}C CP MAS NMR spectra of the adsorbed species obtained after feeding ^{13}C-syngas over ZnAlO$_x$/H-ZSM-5H catalysts at different temperatures: a, 523 K, **b**, 573 K, **c**, 623 K and **d**, 673 K. Reaction conditions: batch reactions for 10 min, H_2/CO=1, 2.5 MPa. Asterisks denote spinning sidebands. More paraffins shown in sharp peaks are observed for reaction at higher temperature, especially at 673 K, where propane (16.6 and 15.5 ppm), n-butane (25.5 and 13.1 ppm) and i-butane (24.0 ppm) with evident signals are labelled[16,17].

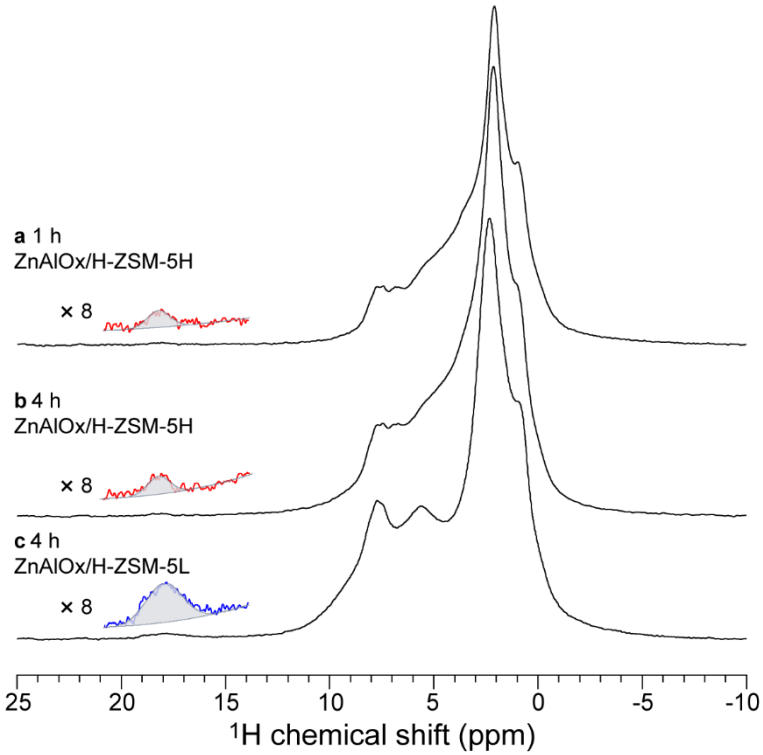

Supplementary Figure 19. Quantification of MCPenones adsorbed on BASs by ^{1}H MAS NMR spectra. Based on our fittings, the amounts of MCPenones adsorbed on the BASs over H-ZSM-5H in $ZnAlO_x$/H-ZSM-5H after **a**, 1 h and **b**, 4 h reaction are both around 11 μmol·g_{zeo}^{-1}, which is consistent with the comparable signal intensity for the peaks of 220-230 ppm in ^{13}C CP MAS NMR spectra (see Figure 2). The amount of MCPenones adsorbed on BASs over H-ZSM-5L in $ZnAlO_x$/H-ZSM-5L after **c**, 4 h reaction is 33 μmol·g_{zeo}^{-1}.

The amounts of MCPenones adsorbed on BASs were calculated by the equation:

$$n_{\mathrm{MCPenone}} = \frac{I_{18\ \mathrm{ppm}}}{I_{\mathrm{ada}}} \times \frac{m_{\mathrm{ada}} \times 16}{0.5 \times m_{\mathrm{sample}} \times M_{\mathrm{ada}}} \qquad (2)$$

where n_{MCPenone} stands for the molar number of MCPenones adsorbed on BASs for 1 g zeolites in composite catalysts, $I_{18\ \mathrm{ppm}}$ for the integral area of ^{1}H MAS NMR signal at around 18 ppm, I_{ada} for the integral area of ^{1}H MAS NMR signal for adamantane, m_{ada} and m_{sample} for the masses of adamantane and samples, respectively, and M_{ada} for molar mass of adamantane (136.23 g·mol^{-1}). The coefficient 0.5 is calculated for the mass ratio of oxides/zeolites = 1:1. In such a calculation, other kinds of adehydes/ketones, adsorbed on BASs forming strong hydrogen bonds with ^{1}H chemical shifts around 18 ppm would also be counted, which would lead to a slight overestimation for the amount of MCPenones adsorbed on the BASs.

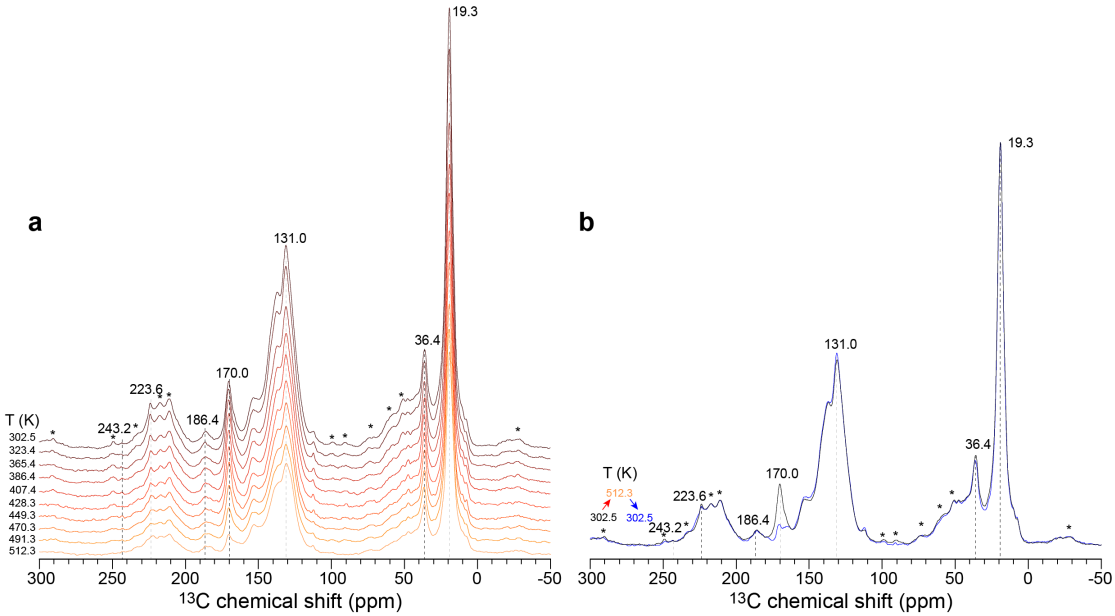

Supplementary Figure 20. The variable-temperature ^{13}C CPSP MAS NMR experiments for ZnAlO$_x$/H-ZSM-5L catalyst after ^{13}C-syngas reaction for 4 h. a, ^{13}C CPSP MAS NMR spectra from 302.5 K to 512.3 K. **b**, ^{13}C CPSP MAS NMR spectra recorded at 302.5 K before and after the variable-temperature experiments. Asterisks denote spinning sidebands.

Supplementary Note 4.

The multi-carbon carboxylates (186.4 ppm), MCPenones (223.6 ppm), and MCPenes$^+$ (243.2 ppm) can be observed over the whole measured temperature range (302.5 - 512.3 K), which proved that these activated species have been captured with no big changes in structure under RT measurement using the quench scheme compared with the high-temperature sampling. Besides, we observed peak broadening for species as multi-carbon carboxylates (186.4 ppm) and MCPenones (223.6 ppm) measured at elevated temperatures, which can be caused by factors including the minor changes in the adsorption structure and dynamics. However, we did not observe unrecognized new species in the VT ssNMR experiments beyond the assigned ones in the RT measurements. A great reduction in the peak intensity of the formate (170.0 ppm) was observed especially when the temperature reached 470.3 K and higher, which was due to the decomposition of formate, supported by the ^{13}C MAS NMR spectra for the same catalyst recorded before and after the VT ssNMR experiments as shown in Figure R1**b**. It is revealed that the decomposition of formate holds a low energy barrier and would occur when there is no gas-phase CO in balance at elevated temperatures.

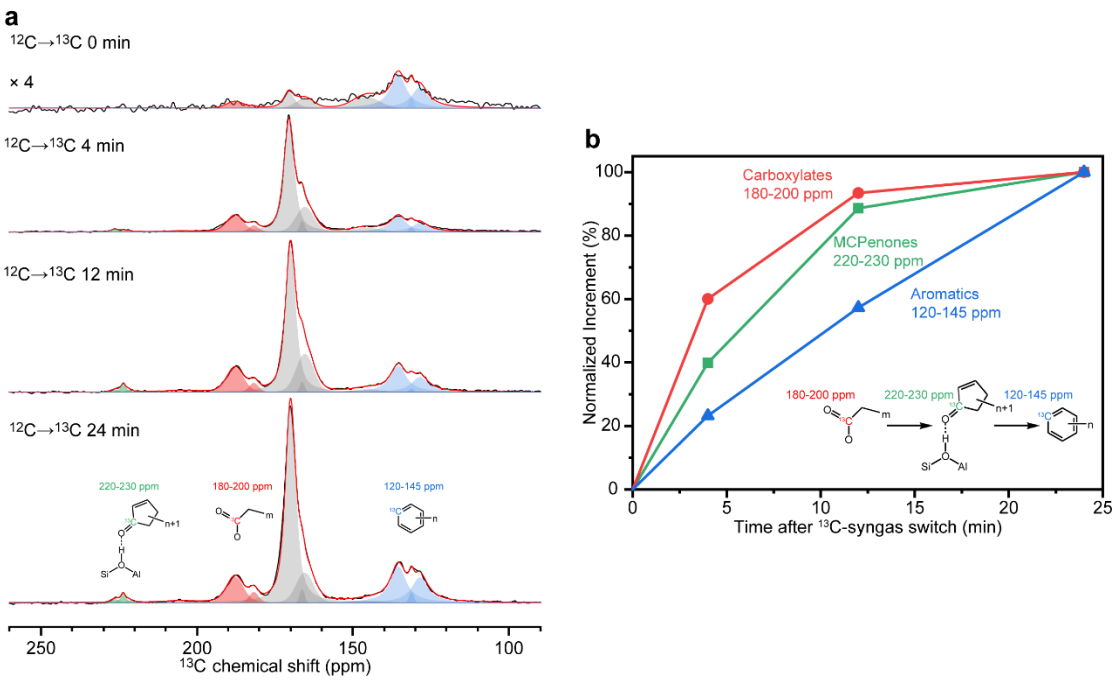

Supplementary Figure 21. The incorporation rate for ^{13}C atoms into different species during the steady-state conversion over $ZnAlO_x$/H-ZSM-5H. a, integral of ^{13}C signals after ^{12}C-^{13}C isotope switch over $ZnAlO_x$/H-ZSM-5H in steady state (Fig. 5**a**). *Green* peaks (221.6, 223.4 and 226.1 ppm): ^{13}C-labelled carbonyl groups in the MCPenones adsorbed on BASs. *Red* peaks (181.7 and 187.7 ppm): ^{13}C-labelled carbonyl groups in the multi-carbon carboxylates. *Blue* peaks (128.7, 131.4 and 135.6 ppm): ^{13}C-labelled carbons in the C=C bonds, mainly from aromatics. *Grey* peaks: other species such as formates. *Black* lines: the original spectra. *Red* lines: the fitting lines. **b**, time evolution for the increment of the ^{13}C-labelled carbonyl groups in the multi-carbon carboxylates (180-200 ppm, *red* circle), ^{13}C-labelled carbonyl groups in the MCPenones (220-230 ppm, *green* square) and ^{13}C-labelled carbons in the C=C bonds which are mainly from aromatics (120-145 ppm, *blue* triangle) after $^{12}C/^{13}C$-syngas isotope switch for 0-24 min. The calculated increments are normalized as [I_i(n min)- I_i(0 min)]/[I_i(24 min)- I_i(0 min)], where I_i(0 min), I_i(24 min) and I_i(n min) correspond to the intensity of the specie i in ^{13}C CP MAS NMR spectra after $^{12}C/^{13}C$-syngas switching for 0, 24 and n min, respectively.

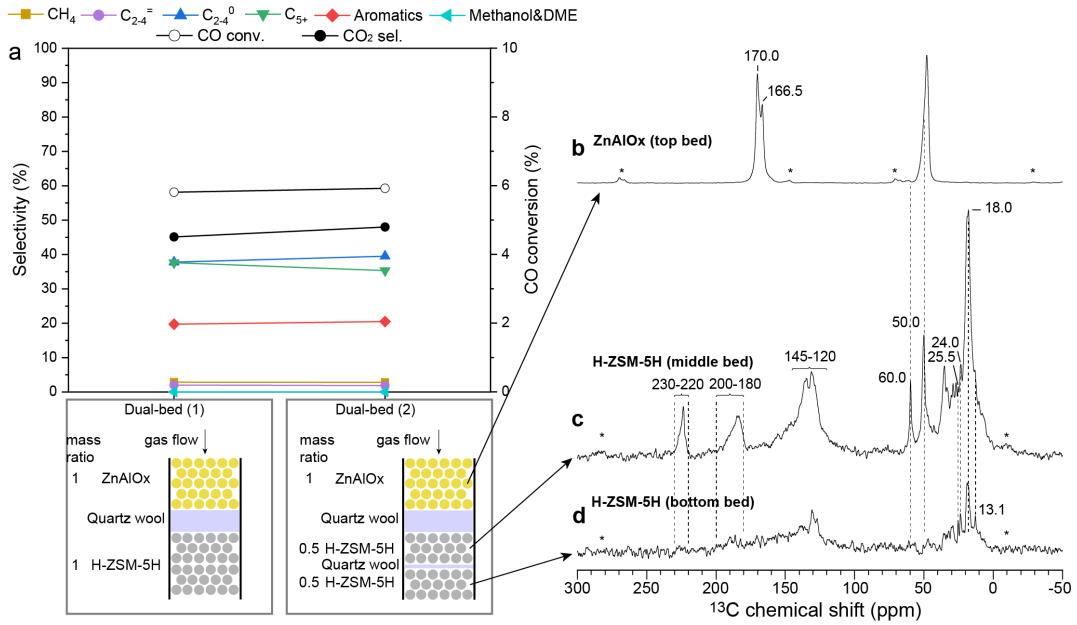

Supplementary Figure 22. The evaluation of intermediate distribution on the dual-bed $ZnAlO_x$-H-ZSM-5H catalyst by ^{13}C isotope tracking experiments during steady-state syngas conversion. a, The catalytic performance of two different dual-bed catalysts, dubbed as (1) and (2). Reaction conditions: 573 K, H_2/CO=1, 2.5 MPa, space velocity = 1000 $ml \cdot h^{-1} \cdot g_{cat}^{-1}$, TOS = 20 h. Selectivities of MeOH, DME and hydrocarbons were calculated on a molar carbon basis by excluding CO_2 in the products. The catalytic performance of dual-bed (1) catalyst is also presented in Supplementary Fig. 11. For dual-bed catalyst (2), the H-ZSM-5H bed is further separated into two beds, which leads to very little changes in the product distribution. ^{13}C CP MAS NMR spectra for the adsorbed species from **b**, the top $ZnAlO_x$ bed (measured at 15 kHz MAS rate), **c**, the middle H-ZSM-5H bed (measured at 22 kHz MAS rate), and **d**, the bottom H-ZSM-5H bed (measured at 22 kHz MAS rate) after ^{13}C syngas isotope switch experiments over dual-bed catalyst (2) for 12 min. Before isotope switch, the reaction has been carried out with natural abundance syngas for 20 h to reach sufficient steady-state conversion. Asterisks denote spinning sidebands.

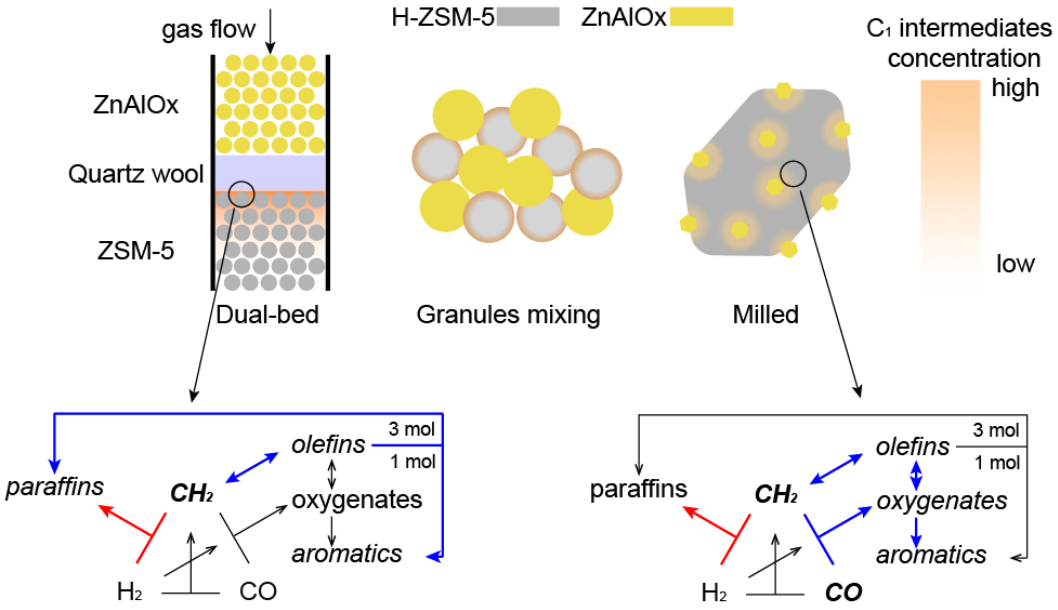

Supplementary Figure 23. Schematic diagram of C_1 intermediate distribution for different $ZnAlO_x$ and H-ZSM-5 mixing modes. The C_1 intermediates (methanol and DME) concentration is shown in *orange* color and the darker color represent a higher concentration.

Supplementary Note 5.

The ^{13}C isotope tracking experiments during steady-state syngas conversion on the dual-bed $ZnAlO_x$-H-ZSM-5H catalyst (Supplementary Fig. 22) revealed a C_1 intermediate concentration gradient in the dual-bed catalyst. The H-ZSM-5H bed in dual-bed (2) catalyst was further separated into two beds using quartz wool, which caused little changes to the catalytic performance (Supplementary Fig. 22**a**). After isotope switch, the $ZnAlO_x$ bed showed signals for formate (~ 170 ppm), methanol (~ 50 ppm) and DME (~ 60 ppm) as expected for the production of C_1 intermediates from metal oxides (Supplementary Fig. 22**b**). Significant differences are observed for the ^{13}C signals from the two beds of H-ZSM-5H. The upper H-ZSM-5 bed (Supplementary Fig. 22**c**) showed the presence of the high concentration of ^{13}C-labelled methanol (~ 50 ppm) and DME (~ 60 ppm), which were not found at the lower H-ZSM-5H bed (Supplementary Fig. 22**d**).

This phenomenon would contribute to the product distribution. On the dual-bed catalyst, there was a high concentration of C_1 intermediates at the top of the inlet side of the H-ZSM-5 bed, where hydrogenation and MTH dominate the product distribution, especially for the hydrogenation reaction leading to much lower selectivity to unsaturated products than solely methanol conversion (Supplementary Fig. 10). On the milled catalysts, the C_1 intermediate concentration was lower and more uniform over the whole catalyst bed, which would help the CO-involved oxygenates-based routes to counter the hydrogenation process and produce more unsaturated products as olefins and aromatics. In addition, the C_1 intermediate distribution can bring useful insights into industrial processes, as the mass transfer mode for the OXZEO catalyst is very different from the typically recognized fix-bed reactor, even though a fix bed is indeed used.

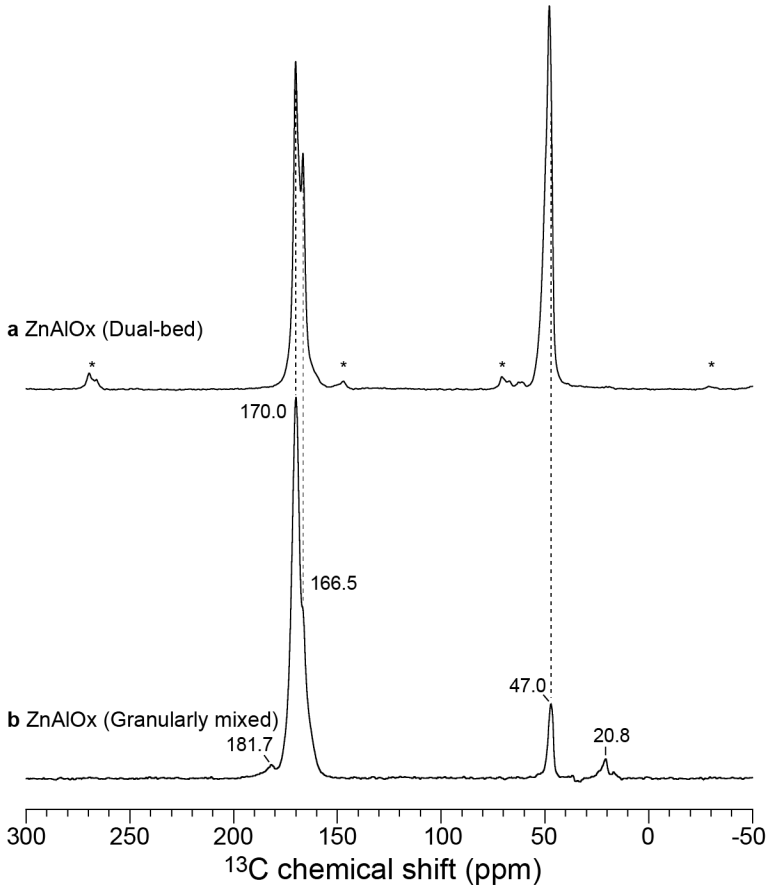

Supplementary Figure 24. Comparison for ^{13}C CP MAS NMR spectra of the $ZnAlO_x$ component in dual-bed and granularly mixed catalysts after ^{13}C-syngas conversion. The spectra are recorded at **a**, 15 kHz MAS rate for $ZnAlO_x$ in dual-bed catalyst (a copy from Supplementary Fig. 22**b**) and **b**, 22 kHz MAS rate for $ZnAlO_x$ in granularly mixed catalyst (a copy from Supplementary Fig. 16**c**), respectively. Asterisks denote spinning sidebands.

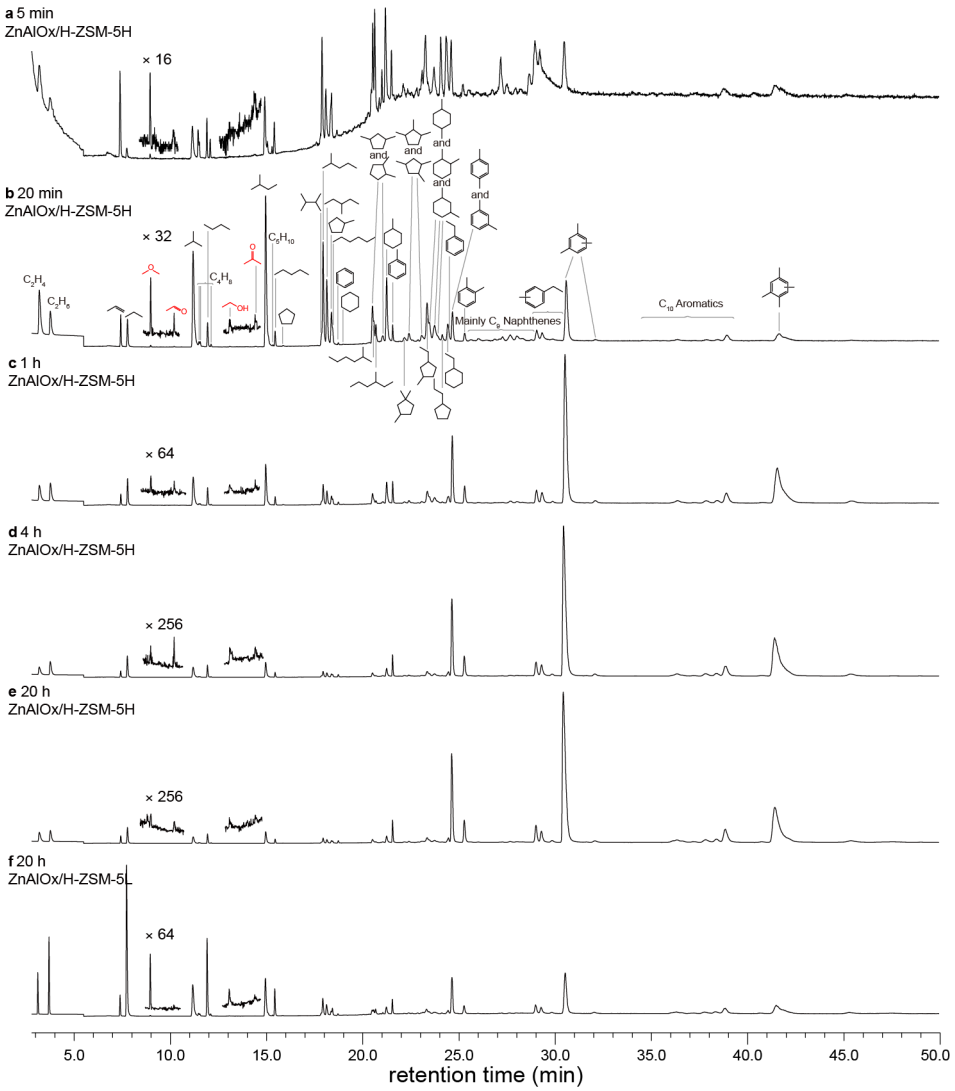

Supplementary Figure 25. GC-MS TICs for the effluent products produced by $ZnAlO_x$/H-ZSM-5 catalysts. syngas conversion over $ZnAlO_x$/H-ZSM-5H for different TOS of **a**, 5min, **b**, 20 min, **c**, 1 h, **d**, 4 h and **e**, 20 h, and ZnAlOx/H-ZSM-5L for **f**, 20 h. Reaction conditions: 573 K, H_2/CO=1, 2.5 MPa, space velocity = 1000 ml·h^{-1}·g_{cat}^{-1}. The m/z detection region was set to 19 - 40 from 2.8 to 5.5 min and switched to 34 - 400 from 5.5 to 50.0 min for a better resolution. Consequently, the signals of methane and methanol were filtered.

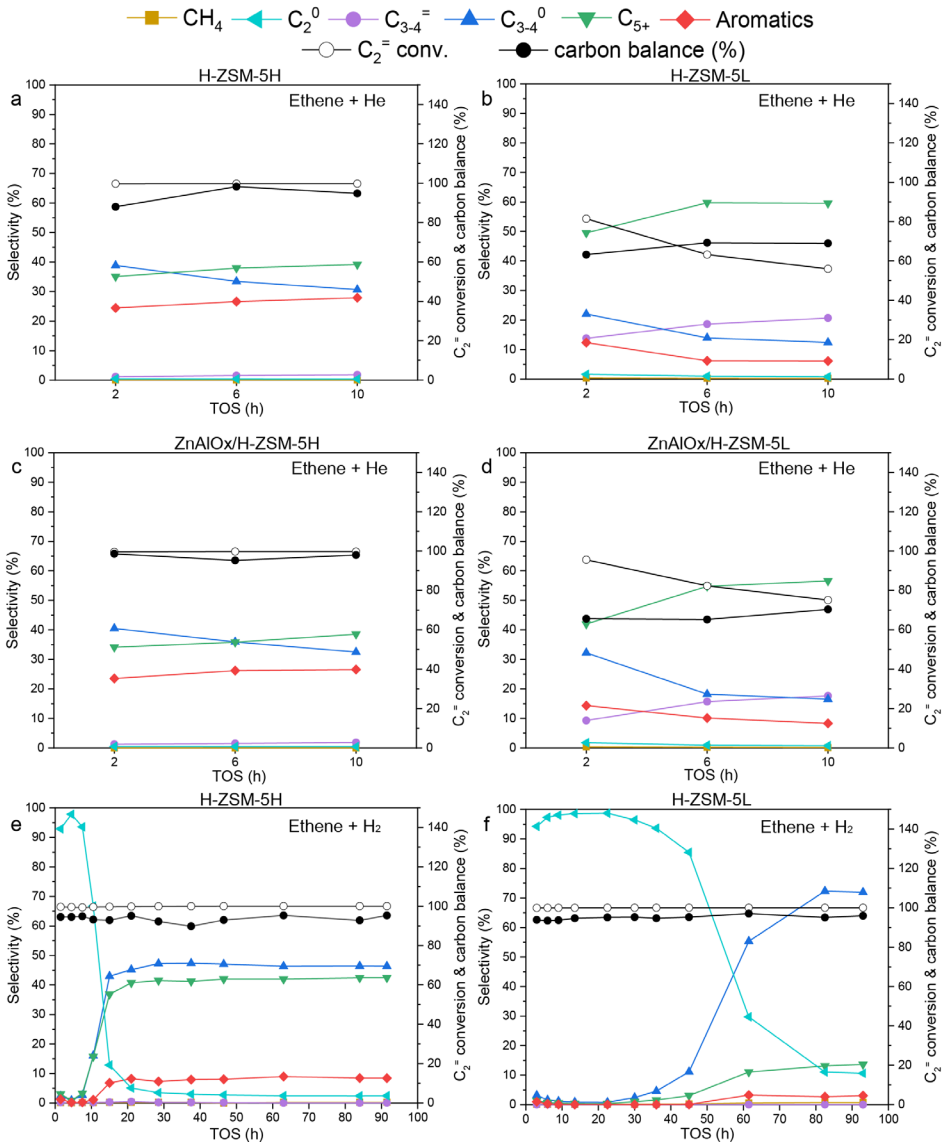

Supplementary Figure 26. Catalytic performance for ethene conversion with He or H_2 cofeeding over H-ZSM-5 and $ZnAlO_x$/H-ZSM-5. Time-on-stream conversion and selectivity of **a**, H-ZSM-5H, **b**, H-ZSM-5L, **c**, $ZnAlO_x$/H-ZSM-5H, and **d**, $ZnAlO_x$/H-ZSM-5L for ethene conversion under He atmosphere. Reaction conditions: 573 K, ethene (4.5 %) + Ar (5 %) balanced with He, 2.5 MPa, space velocity = 1000 $ml/h^{-1}\cdot g_{cat}^{-1}$ for composite catalysts (mass ratio of oxides/zeolites = 1:1) or space velocity = 2000 $ml\cdot h^{-1}\cdot g_{zeo}^{-1}$ for zeolites alone. Time-on-stream conversion and selectivity of **e**, H-ZSM-5H, **f**, H-ZSM-5L for ethene conversion under H_2 atmosphere. Reaction conditions: 573 K, ethene (4.5 %) + Ar (5 %) + H_2 (47.5 %) balanced with He, 2.5 MPa, space velocity = 2000 $ml\cdot h^{-1}\cdot g_{zeo}^{-1}$.

For ethene conversion under He atmosphere over H-ZSM-5H (**a**), the product distribution resembles the one observed for methanol conversion under He (Supplementary Fig. 10**a**), support the operation of classical HT for aromatization under current case. While H-ZSM-5L suffers fast deactivation due to coke formation (**b**). ZnAlOx oxides show little influence on the product selectivity, comparing to sole H-ZSM-5 zeolites (**c**-**d**). When the cofeeding gas is changed from He to H_2, for quite a long time (~ 8 h for H-ZSM-5H; ~ 36 h for H-ZSM-5L) we can only observe ethane as major products (> 90 % selectivity), which is expected to be

produced from the hydrogenation of ethene. Even in prolonged reaction time when aromatic products start to form, however, there are almost no olefins produced on both catalysts and the selectivity to aromatics is extremely low (**e**, ~ 8 % for H-ZSM-5H; **f**, ~ 3 % for H-ZSM-5L). This clearly indicates that the traditional aromatization pathways (aromatization of higher olefins via HT reaction) are severely suppressed with the presence of H_2.

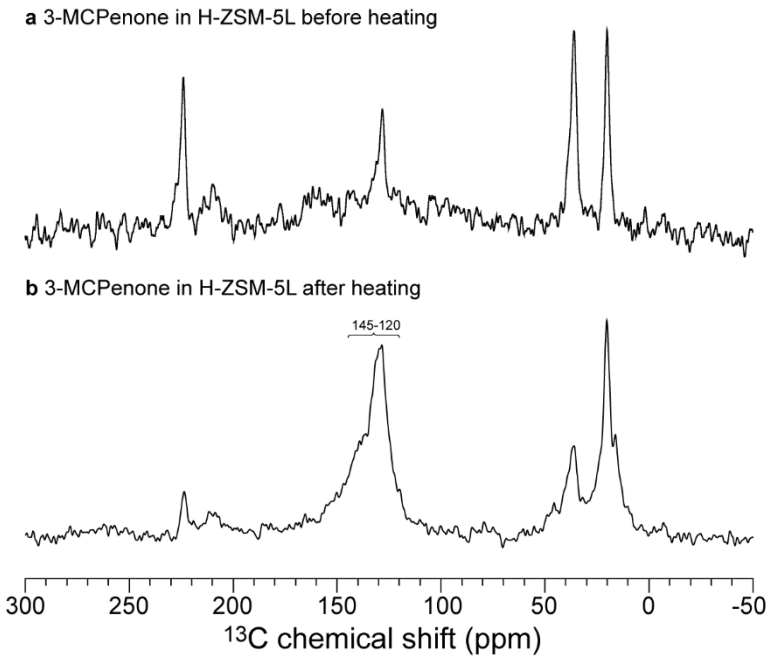

Supplementary Figure 27. Verification of the conversion of MCPenones to aromatics. ^{13}C CP MAS NMR spectra of 3-MCPenone adsorbed in H-ZSM-5L **a**, before and **b**, after heating at 623 K for 3 min in Ar atmosphere. Aromatics identified by the signals range of 120-145 ppm are produced after heating.

Supplementary Table 4. Catalytic performances for syngas conversion over different OXZEO bifunctional catalysts.[a]

Catalysts	SAR[b]	CO conv. (%)	CO_2 sel. (%)	Selectivity (%)[c]									
				MeOH &DME	CH_4	$C_2^=$	C_2^0	$C_3^=$	C_3^0	$C_4^=$	C_4^0	C_{5+}[d]	Aro.
$ZnAlO_x$/H-ZSM-5H	82.4	7.5	45.7	0.2	3.0	3.2	3.9	0.7	4.0	0.2	1.7	6.2	77.0
$ZnAlO_x$/H-ZSM-5L	16.4	7.3	43.7	0.2	5.5	3.8	6.9	1.0	31.4	0.5	11.4	14.1	25.2
$ZnCrAlO_x$/H-ZSM-5H	82.4	10.5	44.7	0.2	4.7	2.5	3.7	0.8	3.4	0.3	2.5	7.3	74.5
$ZnGaO_x$/H-ZSM-5H	82.4	6.8	39.5	0.1	2.2	2.4	1.9	0.5	5.7	0.5	7.9	28.5	50.2
$ZnAlO_x$/H-SSZ-13	14.6	5.9	41.0	11.8	20.0	11.7	7.6	17.6	12.8	4.6	5.1	7.8	1.0
$ZnAlO_x$/H-BETA	12.1	8.4	35.1	1.7	4.1	9.9	7.2	2.5	4.8	0.9	21.6	25.8	21.5

[a]Reaction conditions: $H_2/CO=1$, 2.5 MPa, Space velocity = 1000 $ml \cdot h^{-1} \cdot g_{cat}^{-1}$ for composite catalysts (mass ratio of oxides/zeolites = 1:1). TOS = 20 h. Reactions were performed at 573 K over all catalysts but $ZnCrAlO_x$/H-ZSM-5H where the reaction was performed at 623 K.

[b]The Si/Al ratios (SARs) of different zeolites were measured by ICP-AES.

[c]Selectivities of MeOH, DME and hydrocarbons were calculated on a molar carbon basis by excluding CO_2 in the products.

[d]C_{5+} products except for aromatics.

Supplementary Table 5. Experimental parameters for 1D ssNMR spectra.

Experiment	^{1}H SP	^{1}H-^{13}C CP	^{1}H SP	^{1}H SP	^{13}C SP	^{1}H SP	^{1}H-^{13}C CP
Figure	Fig. S19	Fig. 2, 5 and 7; Fig. S16 and S18	Fig. S4	Fig. S17	Fig. S17	Fig. S17	Fig. S17, S22 and S27
B_0 (T)	14.1	14.1	9.4 (S)[d]	9.4 (L)[d]	9.4 (L)[d]	9.4 (S)[d]	9.4 (S)[d]
MAS (kHz)	22	22	10	static	static	12	12
Recycle delay (s)	5	2	50	5	20	5	2
Number of scans	128	6000-44000	64	32	256	16	7088-15568
^{1}H RF field strength (kHz)	96[a]	76	76[a]	18[e]	N/A	71	71
^{13}C RF field strength (kHz)	N/A	N/A	N/A	N/A	27	N/A	N/A
CP contact time (ms)	N/A	3	N/A	N/A	N/A	N/A	3
^{1}H spinlock field strength (kHz)	N/A	76	N/A	N/A	N/A	N/A	57
^{13}C spinlock field strength (kHz)	N/A	47	N/A	N/A	N/A	N/A	71
^{1}H RF amplitude ramp during spinlock	N/A	Ramp 90 110.1000[b]	N/A	N/A	N/A	N/A	Ramp 90 110.1000[b]
^{1}H decoupling field strength (kHz)	N/A	76[c]	N/A	N/A	3[f]	N/A	71[c]

[a] ^{1}H π/4 pulse was used in ^{1}H SP MAS NMR spectra for quantification.

[b] ^{1}H spin-lock field strength is lineally swept from 90% to 110% in 1000 steps during contact time.

[c] SPINAL64 ^{1}H decoupling

[d] 9.4 (S) stands for a wide-bore Bruker Avance III-400MHz spectrometer equipped with a 4 mm HXY probe. 9.4 (L) stands for a standard-bore Bruker Avance III-400MHz spectrometer equipped with a standard liquid probe.

[e] ^{1}H π/6 pulse was used in ^{1}H SP solution NMR spectra.

[f] waltz16 ^{1}H decoupling.

Supplementary Table 6. Experimental parameters for 2D ssNMR spectra.

Experiment	^{13}C-^{13}C spin-diffusion based correlation	^{13}C-^{13}C spin-diffusion based correlation	$^{13}C\{^{1}H\}$ CP HETCOR	$^{13}C\{^{1}H\}$ CP HETCOR	^{13}C CP refocused INADEQUATE [19]	^{1}H-^{1}H DQ-SQ
Figure	Fig. 3**a**; Fig. S13**a**	Fig. 3**b**; Fig. S13**b**	Fig. 3**c**; Fig. S14**a**	Fig. 3**d**; Fig. S14**b**	Fig. 4	Fig. S15
B_0 (T)	18.8	14.1	18.8	14.1	18.8	14.1
MAS (kHz)	22	22	22	22	22	20
Recycle delay (s)	1.5	1.5	1.5	1.5	1	1.5
Number of scans	800	1024	800	800	4800	128
^{1}H RF field strength (kHz)	56	76	56	76	59	93
^{13}C RF field strength for (kHz)	74	83	N/A	N/A	76	N/A
CP contact time (ms)	3	3	3	3	3	N/A
^{1}H spinlock field strength (kHz)	56	76	56	76	54	N/A
^{13}C spinlock field strength (kHz)	74	47	74	47	76	N/A
^{1}H RF amplitude ramp during spinlock	Ramp 90 110.1000[a]	Ramp 90 110.1000	Ramp 90 110.1000	Ramp 90 110.1000	Ramp 90 110.1000	N/A
Dipolar recoupling scheme	CORDxy4 [18]	CORDxy4	N/A	N/A	N/A	$R12_2^5$
Mixing time (ms)	80	80	N/A	N/A	N/A[b]	0.1[c]
^{1}H RF field strength used in recoupling scheme (kHz)	22 kHz for $R2_1^v$; 11 kHz for $R2_2^v$	22 kHz for $R2_1^v$; 11 kHz for $R2_2^v$	N/A	N/A	N/A	60
^{1}H SPINAL64 decoupling strength (kHz)	56	76	56	76	61	N/A
t_1 sampling points	172	144	144	130	214	164
Δt_1 (μs)	15.15	22.73	45.45	45.45	11.36	50

[a] ^{1}H spin-lock field strength is linely swept from 90% to 110% in 1000 steps during contact time.

[b] The optimized rotor synchronized delay for echoes is 1.5 ms.

[c] Both the DQ excitation and reconversion time are 0.1 ms.

Supplementary References:

1 Schroeder, C. *et al.* Hydrogen Bond Formation of Brønsted Acid Sites in Zeolites. *Chem. Mater.* **32**, 1564-1574 (2020).

2 Schroeder, C., Siozios, V., Hunger, M., Hansen, M. R. & Koller, H. Disentangling Brønsted Acid Sites and Hydrogen-Bonded Silanol Groups in High-Silica Zeolite H-ZSM-5. *J. Phys. Chem. C* **124**, 23380-23386 (2020).

3 Chen, K. *et al.* Direct Detection of Multiple Acidic Proton Sites in Zeolite HZSM-5. *J. Am. Chem. Soc.* **139**, 18698-18704 (2017).

4 Ilias, S. & Bhan, A. Mechanism of the Catalytic Conversion of Methanol to Hydrocarbons. *ACS Catal.* **3**, 18-31 (2013).

5 Mikkelsen, Ø. & Kolboe, S. The conversion of methanol to hydrocarbons over zeolite H-beta. *Microporous Mesoporous Mater.* **29**, 173-184 (1999).

6 Zhang, J. *et al.* Hydrogen transfer versus olefins methylation: On the formation trend of propene in the methanol-to-hydrocarbons reaction over Beta zeolites. *J. Catal.* **368**, 248-260 (2018).

7 Goguen, P. W. *et al.* Pulse-Quench Catalytic Reactor Studies Reveal a Carbon-Pool Mechanism in Methanol-to-Gasoline Chemistry on Zeolite HZSM-5. *J. Am. Chem. Soc.* **120**, 2650-2651 (1998).

8 Yang, L. *et al.* Role of acetaldehyde in the roadmap from initial carbon-carbon bonds to hydrocarbons during methanol conversion. *ACS Catal.* **9**, 6491–6501 (2019).

9 Xu, M., Wang, W. & Hunger, M. Formation of acetone enol on acidic zeolite ZSM-5 evidenced by H/D exchange. *Chem. Commun.*, 722-723 (2003).

10 Wang, Z., Heising, J. M. & Clearfield, A. Sulfonated Microporous Organic−Inorganic Hybrids as Strong Bronsted Acids1. *J. Am. Chem. Soc.* **125**, 10375-10383 (2003).

11 Biaglow, A. I., Sepa, J., Gorte, R. J. & White, D. A ^{13}C NMR Study of the Condensation Chemistry of Acetone and Acetaldehyde Adsorbed at the Brønsted Acid Sites in H-ZSM-5. *J. Catal.* **151**, 373-384 (1995).

12 Chowdhury, A. D. *et al.* Initial Carbon-Carbon Bond Formation during the Early Stages of the Methanol-to-Olefin Process Proven by Zeolite-Trapped Acetate and Methyl Acetate. *Angew. Chem. Int. Ed.* **55**, 15840-15845 (2016).

13 Fu, D. *et al.* Elucidating Zeolite Channel Geometry–Reaction Intermediate Relationships for the Methanol-to-Hydrocarbon Process. *Angew. Chem. Int. Ed.* **59**, 20024-20030 (2020).

14 Gao, P. *et al.* A Mechanistic Study of Methanol-to-Aromatics Reaction over Ga-Modified ZSM-5 Zeolites: Understanding the Dehydrogenation Process. *ACS Catal.* **8**, 9809-9820 (2018).

15 Xiao, D. *et al.* Direct structural identification of carbenium ions and investigation of host–guest interaction in the methanol to olefins reaction obtained by multinuclear NMR correlations. *Chem. Sci.* **8**, 8309-8314 (2017).

16 Chen, Y. *et al.* C−C Bond Formation in Syngas Conversion over Zinc Sites Grafted on ZSM-5 Zeolite. *Angew. Chem. Int. Ed.* **59**, 6529-6534 (2020).

17 Ivanova, I. I., Pomakhina, E. B., Rebrov, A. I. & Derouane, E. G. ^{13}C MAS NMR mechanistic study of the initial stages of propane activation over H-ZSM-5 zeolite. *Top. Catal.* **6**, 49 (1998).

18 Hou, G., Yan, S., Trébosc, J., Amoureux, J.-P. & Polenova, T. Broadband Homonuclear Correlation Spectroscopy Driven by Combined $R2_n^v$ Sequences under Fast Magic Angle Spinning for NMR Structural Analysis of Organic and Biological Solids. *J. Magn. Reson.* **232**, 18-30 (2013).

19 Lesage, A., Bardet, M. & Emsley, L. Through-bond carbon-carbon connectivities in

disordered solids by NMR. *J. Am. Chem. Soc.* **121**, 10987-10993 (1999).